RSC Advances

PAPER

View Article Online
View Journal | View Issue

Cite this: *RSC Adv.*, 2020, **10**, 17816

Synthesis, characterization and corrosion inhibition behavior of 2-aminofluorene bis-Schiff bases in circulating cooling water†

Wenchang Wei,[a] Zheng Liu,*[a] Chuxin Liang,[a] Guo-Cheng Han,*[b] Jiaxing Han[a] and Shufen Zhang[abc]

In this work, two new bis-Schiff bases, namely 2-bromoisophthalaldehyde-2-aminofluorene (**M1**) and glutaraldehyde 2-aminofluorene (**M2**), were synthesized, and their structures were characterized and confirmed by infrared spectroscopy, Fourier transform mass spectrometry and UV-visible spectroscopy. Their corrosion inhibition performance on carbon steel in simulated circulating cooling water was investigated by weight loss measurements and electrochemical measurements. The potentiodynamic polarization curves confirmed that two bis-Schiff bases are anode-type inhibitors; electrochemical impedance spectroscopy tests showed that **M1** and **M2** possess the best inhibition efficiencies of 96.25% and 99.15% at the optimal concentration of 2.50 mmol L^{-1}, respectively. The weight loss results showed that **M1** and **M2** exhibit maximum η_w values of 92.62% and 96.31%, respectively. Scanning electron microscopy showed that the inhibitors inhibited carbon steel corrosion. The adsorption isotherm measurements indicated that the two inhibitors exhibited physicochemisorption mechanisms and followed Langmuir adsorption isotherms. The relationships between the molecular structure and inhibition behavior of the inhibitors were explored by density functional theory, frontier molecular orbital studies, and Fukui index analysis, which affirmed that **M2** possesses higher corrosion inhibition efficiency than **M1**.

Received 28th February 2020
Accepted 18th April 2020

DOI: 10.1039/d0ra01903h

rsc.li/rsc-advances

1. Introduction

Metals are the most widely used engineering materials in modern society; however, metals tend to react with surrounding media, resulting in metal corrosion. In most cases, the metal corrosion starts from the surface and gradually extends to the interior and entirety of the metal. Metal corrosion not only seriously affects the national economy but also causes serious safety hazards and a series of environmental pollution problems.[1–4] Increasing numbers of diverse anticorrosive measures are being studied for metal protection, such as alloy substitution, coating protection, electrochemical protection, and addition of inhibitors.[5–8] Compared with other methods, addition of inhibitors to the corrosive medium is an anti-corrosion method with a simple process, low cost and remarkable effects. Although many inhibitors have good inhibition properties, they are unable to meet the needs of environmental protection and sustainable development strategies for various reasons (such as difficulty in degradation, toxicity or high temperature resistance). Stable, efficient and environmentally friendly inhibitors are the future direction of inhibitor development. There are many kinds of inhibitors, such as imidazolines,[9] Mannich bases,[10,11] quaternary ammonium salts,[12,13] acetylene alcohols, pyridines,[14] and Schiff bases.[15,16] These inhibitors contain heteroatoms (N, S, O) or electron-rich chemical bonds (π bonds).[17–20] The bis-Schiff base compounds contain N, O, and S heteroatoms and unsaturated C=N bonds, which can form strong and stable corrosion-inhibiting adsorption films on metal surfaces, exhibiting excellent inhibition effects. At the same time, Schiff base compounds have the characteristics of low cost, facile synthesis and purification, good water solubility, and non-toxicity, which are favored by researchers.[21–23]

Research on Schiff base inhibitors is prevalent; however, there are few studies on the application of Schiff base inhibitors in circulating cooling water. Circulating cooling water is a major item in industrial water. In the petrochemical electric power, steel, metallurgical and other industries, the amount of circulating cooling water accounts for 50–90% of the total water consumption of enterprises.[24–27] There are many corrosive substances in circulating cooling water, such as chloride ions, sulfate ions, and microorganisms. When the cooling water is continuously circulated in the circulation system, the water temperature will rise and the water will evaporate; this will

[a]*College of Chemical and Biological Engineering, Guilin University of Technology, Guangxi Key Laboratory of Electrochemical and Magneto-chemical Functional Materials, Guilin 541004, P. R. China. E-mail: lisa4.6@163.com*

[b]*School of Life and Environmental Sciences, Guilin University of Electronic Technology, Guilin, 541004, P. R. China. E-mail: hangc81@guet.edu.cn*

[c]*Key Laboratory of Fine Chemicals, Dalian University of Technology, Dalian 116024, P. R. China*

† Electronic supplementary information (ESI) available. See DOI: 10.1039/d0ra01903h

increase the concentration of the corrosive medium and erode the cooling equipment, leading to equipment corrosion and perforation and the formation of leaks, which create safety risks during industrial production. For equipment corrosion, inhibitors such as mercaptobenzothiazole (MBT) and benzotriazole (BTA) are usually added to the circulating cooling water.[28–31] Inhibitors can form a corrosion-inhibiting film on the metal surface to inhibit the corrosion of metals by corrosive media. Because the inhibitor does not need to be added in a large amount, does not require special equipment, and does not need to be pre-treated, it is an economical metal corrosion protection technology. Therefore, the addition of an inhibitor to circulating cooling water is the preferred method to prevent harmful ions from corroding equipment.[32–34] Currently, it is urgent to design and synthesize corrosion inhibitor molecules with higher corrosion inhibition efficiency.[35,36] Therefore, research in the field of circulating cooling water inhibitors in industrial production plants is increasingly valued and favored by researchers. For different water quality and different test conditions, the following problems should be considered when synthesizing inhibitors: (a) increase in the concentration ratio of circulating cooling water by the inhibitor; (b) effective alleviation of the corrosion of metal pipes; (c) less environmental pollution.[34]

Herein, 2-bromoisophthalaldehyde-2-aminofluorene (**M1**) and glutaraldehyde 2-aminofluorene (**M2**) inhibitors were studied by electrochemical measurements, weight loss measurements, scanning electron microscopy and energy dispersive spectrometry in simulated circulating cooling water. Quantum chemical calculation studies were also used to study the corrosion inhibiting properties of the inhibitor molecules. Afterwards, the structural parameters of the inhibitors were also calculated by DFT, mainly including the electronegativity, HOMO, LUMO, chemical softness, chemical hardness, and maximum electron numbers transferred in the chemical reactions of the inhibitors. We also aimed to study the effects of the structural parameters of the inhibitors on their inhibitory effects through quantum chemical calculations and to study their adsorption mechanisms on the metal surface. We hoped to identify the inhibitor with the best corrosion inhibition performance between 2-bromoisohthalaldehyde-2-aminofluorene (**M1**) and glutaraldehyde 2-aminofluorene (**M2**) through these studies, which would be the most suitable for protecting circulating cooling water systems.

2. Experimental

2.1 Materials and solutions

In this study, all the required chemicals and solvents were analytical grade, such as 2-aminofluorene, 2-bromoisophthalaldehyde, glutaraldehyde, methanol, and acetonitrile; these were purchased from Aladdin and used without further purification. The composition of the carbon steel specimens (weight%) was 4.51% C, 0.37% Si, 26.37% O, 1.36% Cr and remainder Fe. The specimens were sanded with 400, 800, and 1200 emery paper until smooth, then cleaned with distilled water and ethanol[37] and dried by cold air; then, the non-working surfaces were sealed with molten paraffin, wrapped in filter paper, and weighed three times before use to obtain the average value. Simulated circulating cooling water was prepared in the laboratory (according to the standards adopted by the American Society for Testing and Materials)[38] for all studies; its properties are shown in Table 1.

2.2 Synthesis of bis-Schiff base inhibitors

2-bromoisophthalaldehyde-2-aminofluorene (**M1**) and glutaraldehyde 2-aminofluorene (**M2**) were synthesized by solution methods.[39–41] The raw materials were dissolved by ultrasonic vibration and refrigerated until use. To prepare **M1**, 2-aminofluorene (2.2 mM) and 2-bromoisophthalaldehyde (1.0 mM) were dissolved in 25 mL absolute ethanol and were placed in a three-necked flask (50 mL); then, 1 mL acetic acid was added. The three-necked flask was placed in a constant temperature water bath and magnetically stirred at a constant speed; the temperature was set to 45 °C, and nitrogen protection was performed. The products were washed three times with ethanol and dried in vacuum. Similarly, **M2** was synthesized from 2-aminofluorene (2.2 mM) and glutaraldehyde (1.0 mM). The synthesis route and molecular structure of **M1** and **M2** are shown in Scheme 1.

Next, **M1** and **M2** were characterized by elemental analysis, FTIR spectroscopy, FTMS and UV-vis spectroscopy.

For **M1**, yield: 78.36%, elemental analysis: anal. calcd: 75.55; H, 4.63; N, 5.18; found: C, 75.50; H, 4.58; N, 5.12%; characteristic IR peaks (KBr disk): ν C–H (aromatic) = 2919, ν C=O = 1616, ν C=N = 1458 cm^{-1} (ref. 42) (in Fig. S1†); FTMS **M1** + H^+: 539.11 amu in Fig. S2;† characteristic UV-vis peaks, C=O (n–π^* transition) = 280, 363 nm in Fig. S3.†

For **M2**, yield: 82.51%, elemental analysis: anal. calcd: 89.39; H, 5.30; N, 5.31; found: C, 89.34; H, 5.27; N, 5.30%; characteristic IR peaks (KBr disk): ν C–H (aromatic) = 2933, ν C=O = 1592, ν C=N = 1454 cm^{-1} [42] (in Fig. S1†); FTMS **M1** + H^+: 527.22 amu in Fig. S2;† characteristic UV-vis peaks, C=O (n–π^* transition) = 315 nm in Fig. S3.†

2.3 Weight loss (WL) measurements

Treated carbon steel specimens were immersed in simulated circulating cooling water with and without addition of different concentrations of **M1** and **M2** for 48 h at 25 °C, respectively. Each concentration was tested three times in parallel, and the

Table 1 The composition of the simulated circulating cooling water

Composition	NaCl	$MgCl_2$	Na_2SO_4	$CaCl_2$	$NaHCO_3$	KBr	H_3BO_3
g L^{-1}	29.06 ± 0.81	10.4 ± 0.24	8.18 ± 0.10	2.32 ± 0.18	0.402 ± 0.013	0.202 ± 0.011	0.054 ± 0.004

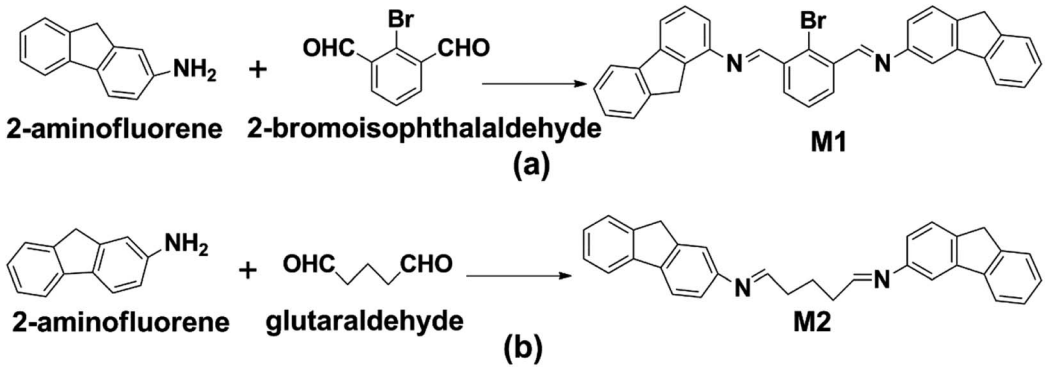

Scheme 1 The synthesis routes of (a) 2-bromoisophthalaldehyde-2-aminofluorene (**M1**), (b) glutaraldehyde-2-aminofluorene (**M2**).

best results were chosen. The following equations were used to calculate the inhibition efficiency (η_w, %):[43–45]

$$\Delta W = W_0 - W_1 \quad (1)$$

$$A = \frac{\Delta W}{St} \quad (2)$$

$$\theta = \frac{i^o_{corr} - i_{corr}}{i^o_{corr}} \quad (3)$$

$$\eta_w\,(\%) = \theta \times 100 \quad (4)$$

where W_0 and W_1 are the average weight losses (g) of carbon steel sheets in simulated circulating cooling water without and with addition of **M1** and **M2**, respectively.[46–48] S is the total area of the carbon steel immersed in the simulated circulating cooling water (cm^2), t is the immersing time (h), θ is the surface coverage, and i^o_{corr} and i_{corr} are the corrosion rates (g cm^{-2} h^{-1}) of the carbon steel sheet in the simulated circulating cooling water without and with addition of **M1** and **M2**, respectively. Furthermore, in order to study the effects of temperature on the inhibition efficiency, the carbon steel sheet was immersed in simulated circulating cooling water containing 2.5 mmol L^{-1} inhibitor at different temperatures for 48 h.

2.4 Electrochemical measurements

The performance of the inhibitors was evaluated on a CHI860D electrochemical workstation with a classical three-electrode system.[36] Before the experiment, the working electrode was plugged into simulated circulating cooling water for 25 min to obtain a stable open circuit potential (OCP); the scanning rate was 1 mV s^{-1} and the potential was ±400 mV for the potentiodynamic polarization (PDP) curves. The angular frequency range was 10^5 Hz to 10^2 Hz, and the sensitivity was automatically adjusted. Electrochemical impedance spectroscopy (EIS) was performed by a sine wave with 5 mV signal amplitude; the frequency range was 1 MHz to 100 kHz. Each concentration was tested three times in parallel.

The corrosion inhibition efficiency η_{PDP} (%) (calculated by the PDP parameters) and η_z (%) (calculated by the EIS parameters)[49] were determined using the following equations, respectively:

$$\eta_{PDP}\ (\%) = \left(\frac{I^o_{corr} - I^i_{corr}}{I^o_{corr}}\right) \times 100 \quad (5)$$

$$\eta_z\ (\%) = \left(\frac{R_{ct} - R^o_{ct}}{R_{ct}}\right) \times 100 \quad (6)$$

where R_{ct} and R^o_{ct} are the charge transfer resistances of carbon steel with and without addition of **M1** and **M2** in simulated circulating cooling water, respectively; I^i_{corr} and I^o_{corr} are the corrosion current densities (μA cm^{-2}), respectively.

2.5 SEM and EDS studies

A scanning electron microscope (S4800) was used to observe the surface morphologies of the carbon steel specimens after immersion in simulated circulating cooling water with and without inhibitor for 24 h, and we compared the polished specimens to analyze the corrosion inhibition effects of the inhibitors. The test magnification was 1000 times and the acceleration voltage was 5.0 kV. A Bruker XFlash 6 | 10 energy spectrometer was used to perform elemental analysis on the surfaces of carbon steel samples immersed in simulated circulating cooling water containing the corrosion inhibitors.

2.6 Quantum chemical calculation studies

Due to its combination of chemistry and computation, the content of computational chemistry research is increasingly rich. Quantum chemical calculations are gaining increasing attention in the study of inhibition mechanisms.[50–53] The molecular structures and electronic parameters of the inhibitors were studied to determine their adsorption behavior on carbon steel. Density functional theory (DFT) is a quantum chemical calculation method with high accuracy when calculating the molecular structure parameters of inhibitors,[54] mainly including electronegativity, frontier orbitals (HOMO and LUMO), chemical softness, chemical hardness, maximum electron number transferred in the chemical reaction, *etc.*[55] Through these structural parameters, the structure–activity relationships of inhibitors can be explored from the perspective of microscopic observation, the mechanisms of the inhibitors can be revealed, and theoretical guidance can be provided for the design and synthesis of new inhibitors. All the structural

parameter calculations were derived from the Gaussian 09 program;[56–58] the optimized molecular structures were mapped by the GaussView 05 program, the Fukui function was obtained from the Multiwfn program,[59] and the Fukui function[60,61] was visualized by the GaussView 05 program. All geometric configuration optimization and quantum chemical calculations were carried out in the gas phase using the B3LYP\6-311+G(d, p) method.[62]

The electronegativity (χ),[63,64] chemical hardness (η),[65] chemical softness (σ),[66] and maximum electrons transferred were calculated by eqn (7)–(10), respectively:

$$\chi \approx -\frac{1}{2}(E_{\mathrm{HOMO}} + E_{\mathrm{LUMO}}) \quad (7)$$

$$\eta \approx -\frac{1}{2}(E_{\mathrm{HOMO}} - E_{\mathrm{LUMO}}) \quad (8)$$

$$\sigma \approx -2/(E_{\mathrm{HOMO}} - E_{\mathrm{LUMO}}) \quad (9)$$

$$\Delta N_{\max} = \frac{\chi}{2\eta} \quad (10)$$

The Fukui function can be used to predict the active site of the inhibitor in an electrophilic substitution reaction. The Fukui function provides information about the sites in the molecule where atoms may be attacked by electrophiles and the sites in the molecule where atoms may be attacked by nucleophiles.

The Fukui functions of the inhibitor molecules were obtained from the following equations:

$$f^{+} = q_{(N+1)} + q_N \quad (11)$$

$$f^{-} = q_{(N)} + q_{(N-1)} \quad (12)$$

where q is the electronic density of the molecule. $q_{(N+1)}$, q_N and $q_{(N-1)}$ are the atomic charges in a system with $N+1$, N and $N-1$ electrons, respectively.[67]

3. Results and discussion

3.1 Weight loss (WL) analysis

If a metal is corroded by corrosive media, it will lose weight. Circulating cooling water has a relatively high salt content, and it contains a large number of free chloride ions and corrosive substances which can cause metal equipment to lose weight due to corrosion. Therefore, the anti-corrosive behavior of the inhibitor molecules on carbon steel in simulated circulating cooling water was studied by WL measurements. Furthermore, the results obtained from the WL measurements are often in agreement with the results of electrochemical analysis.[68] The corrosion inhibition efficiency η_w (%) and WL parameters are listed in Table 2. The weight loss of carbon steel decreased with increasing inhibitor concentration. When the inhibitor concentration was 2.50 mmol L^{-1}, **M1** and **M2** exhibited maximum η_w (%) values of 92.62% and 96.31%, respectively. The corrosion inhibition efficiencies of **M1** and **M2** at different temperatures are listed in Table 3. If the adsorption mechanism of the corrosion inhibitor on the metal surface is physical adsorption, the inhibitor will gradually weaken or disappear as the temperature increases. However, the results showed that

Table 2 Weight loss parameters of carbon steel corrosion in simulated circulating cooling water for 48 h without and with different concentrations of **M1** and **M2** at 25 °C

Inhibitor	C (mmol L^{-1})	ΔW (g)	A (g m^{-2} h^{-1})	θ	η_w (%)
Blank	0	0.514 ± 0.014	25.73 ± 0.43	—	—
M1	0.05	0.189 ± 0.013	7.35 ± 0.16	0.6322	63.22
	0.10	0.128 ± 0.010	6.40 ± 0.08	0.7512	75.12
	0.50	0.088 ± 0.009	4.40 ± 0.10	0.8289	82.89
	1.00	0.056 ± 0.005	2.05 ± 0.06	0.8912	89.12
	2.50	0.038 ± 0.005	1.90 ± 0.04	0.9262	92.62
M2	0.05	0.195 ± 0.015	7.70 ± 0.19	0.6206	62.06
	0.10	0.125 ± 0.012	6.25 ± 0.11	0.7571	75.71
	0.50	0.061 ± 0.010	3.05 ± 0.06	0.8815	88.15
	1.00	0.045 ± 0.009	2.25 ± 0.04	0.9125	91.25
	2.50	0.019 ± 0.005	0.95 ± 0.03	0.9631	96.31

Table 3 Corrosion inhibition behavior of carbon steel in simulated circulating cooling water for 48 h with 2.50 mmol L^{-1} **M1** and **M2** at different temperatures

	A (g m^{-2} h^{-1})				η_w (%)			
Inhibitor	25 °C	35 °C	45 °C	55 °C	25 °C	35 °C	45 °C	55 °C
Blank	25.73 ± 0.13	28.67 ± 0.19	44.67 ± 0.38	63.62 ± 0.51				
M1	1.89 ± 0.05	3.14 ± 0.09	5.69 ± 0.11	9.06 ± 0.22	92.62	89.04	87.26	85.75
M2	0.95 ± 0.04	2.10 ± 0.06	4.55 ± 0.12	7.87 ± 0.18	96.31	92.68	89.81	87.63

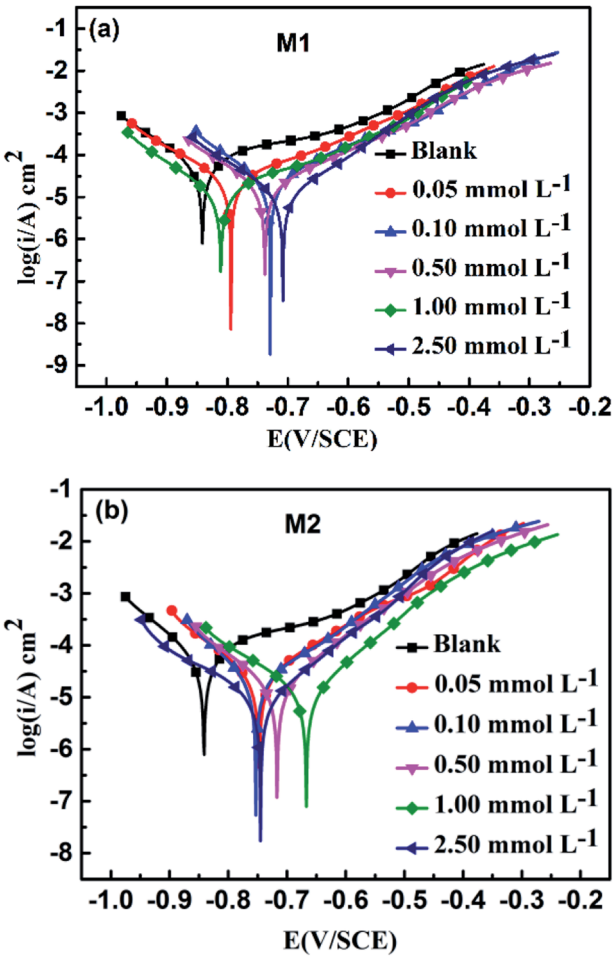

Fig. 1 Potentiodynamic polarization curves for carbon steel in simulated circulating cooling water in the absence and presence of different concentrations of M1 (a) and M2 (b).

with increasing temperature, the corrosion rates did not decrease significantly; this indicates that the adsorption of the corrosion inhibitors onto the metal surface may occur by physicochemical adsorption (mainly chemical adsorption), which can effectively inhibit the corrosion of low-carbon steel.

The weight loss experiment results showed that **M2** possesses better corrosion inhibition performance. This may be because the **M2** structure has good planarity and the structure contains fewer hydrophobic benzene rings; thus, **M2** is more soluble and more easily adsorbed on the carbon steel surface.

3.2 Potentiodynamic polarization curve analysis

The corrosion process of carbon steel mainly involves anodic dissolution and cathodic reduction.[69] The PDP curves for carbon steel without and with addition of **M1** and **M2** in simulated circulating cooling water at 25 °C are displayed in Fig. 1. The potentiodynamic polarization curves show that **M1** and **M2** have the same trend as the polarization curves of the blank group (without inhibitor); this reveals that addition of the inhibitors does not change the corrosion mechanism of carbon steel.[70] Both inhibitors have the same corrosion inhibition process. Compared with the blank group, the current densities of the anode and the cathode of the specimens with the inhibitors were low, showing the inhibitory effect. The dynamic potential parameters obtained from the experiments, including the Tafel slopes of the anode and cathode (β_a and β_c) and the calculated corrosion inhibition rates (η_{PDP}, %), are shown in Table 4. When the inhibitors were added, the η_{PDP} (%) increased, and the highest η_{PDP} (%) values were 83.14% and 85.94% at the maximum concentration (2.50 mol L^{-1}) for **M1** and **M2**, respectively. It can be clearly seen from Table 4 that the changes of β_a and β_c are not obvious when compared with the blank group data; this indicates that the inhibitor molecules are adsorbed on the surface of carbon steel to reduce the number of active centers of the metal surface rather than by changing the anode and cathode mechanism to inhibit corrosion.[48,71]

3.3 EIS analysis

EIS was used to explore the electrode process dynamics and surface phenomena at the metal-solution interface.[35] The Nyquist and Bode diagrams obtained from EIS studies of carbon steel with different concentrations of **M1** and **M2** at 25 °C are displayed in Fig. 2. The generation of the capacitive anti-arc is the result of the formation of an adsorption film on the carbon steel surface by the inhibitor and the resistance of the charge

Table 4 Potentiodynamic polarization curve (PDP) parameters for carbon steel in simulated circulating cooling water without and with different concentrations of M1 and M2 at 25 °C

Inhibitor	Conc. (mmol L^{-1})	$-E_{corr}$ (mV)/SCE	I_{corr} (μA cm^{-2})	β_a (mV dec^{-1})	$-\beta_c$ (mV dec^{-1})	η (%) (PDP)
Blank	0	841 ± 27	74.2 ± 8.4	3.43 ± 0.50	9.09 ± 0.52	—
M1	0.05	794 ± 22	34.9 ± 4.1	4.73 ± 0.51	7.59 ± 0.48	52.93
	0.10	729 ± 24	24.7 ± 2.1	6.71 ± 0.82	10.18 ± 0.59	66.72
	0.50	738 ± 21	20.1 ± 2.2	6.46 ± 0.91	8.77 ± 0.53	72.99
	1.00	811 ± 25	15.5 ± 1.1	4.43 ± 0.63	9.40 ± 0.59	79.09
	2.50	708 ± 21	12.5 ± 1.0	8.59 ± 0.70	9.04 ± 0.60	83.14
M2	0.05	747 ± 23	28.2 ± 2.3	6.82 ± 0.62	8.14 ± 0.55	61.98
	0.10	753 ± 19	21.5 ± 1.7	6.78 ± 0.84	10.66 ± 0.64	71.05
	0.50	717 ± 24	16.8 ± 1.3	8.10 ± 0.71	8.85 ± 0.58	77.38
	1.00	667 ± 20	13.4 ± 1.3	6.80 ± 0.57	9.47 ± 0.51	81.91
	2.50	745 ± 22	10.4 ± 1.1	5.65 ± 0.51	9.07 ± 0.59	85.94

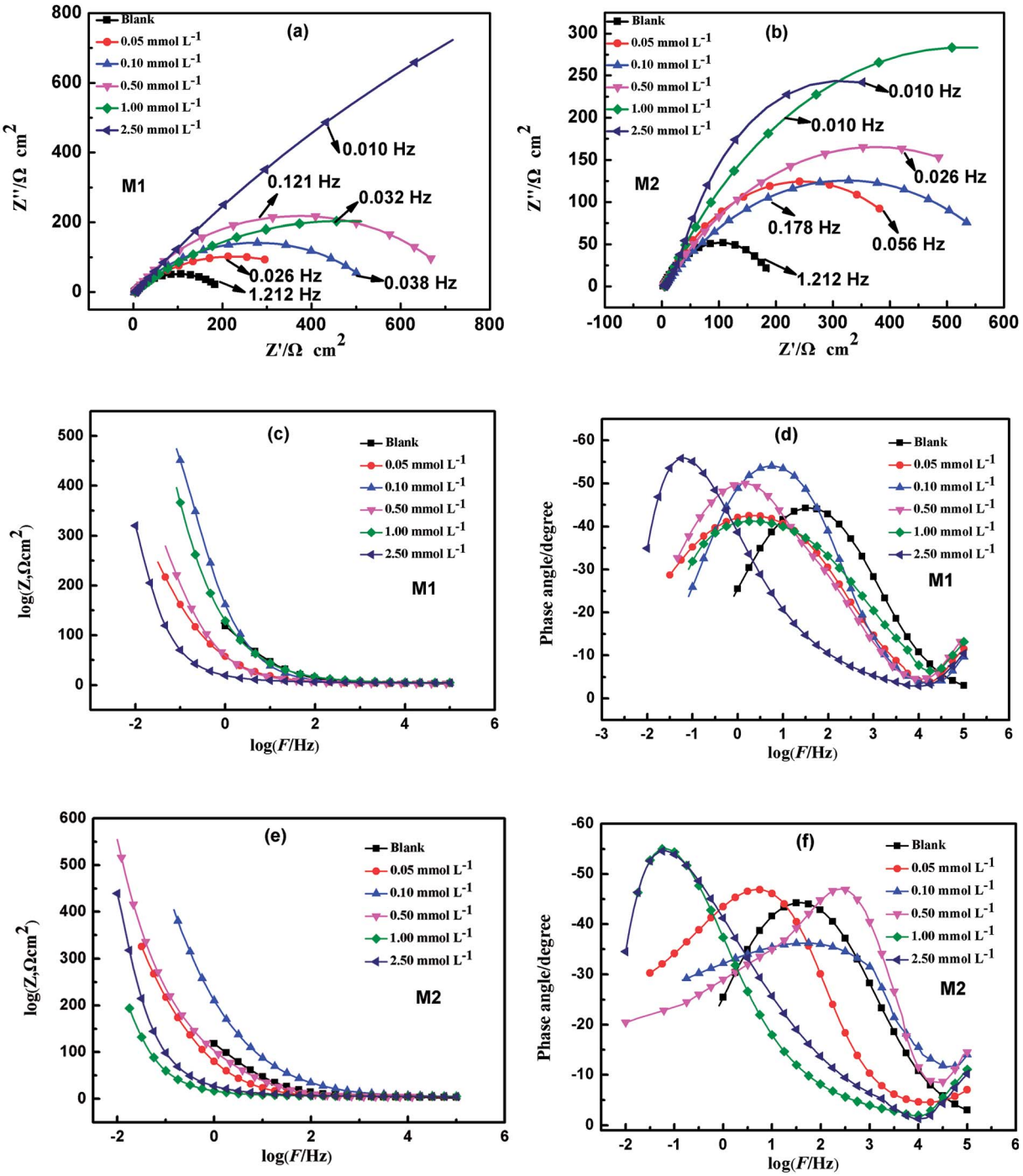

Fig. 2 Nyquist (a and b), Bode (c and e) and phase angle diagrams (d and f) for carbon steel in simulated circulating cooling water in the absence and presence of different concentrations of M1 and M2.

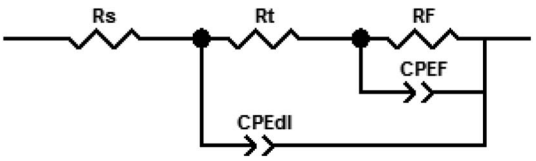

Fig. 3 Electrical equivalent circuit used to fit the EIS data.

transfer.[49] The Nyquist diagrams show that in the simulated circulating cooling water, the diameters of the capacity arcs of the specimens with the inhibitors were larger than that of the carbon steel without inhibitor, which indicates that the corrosion reaction was inhibited. The corrosion inhibition efficiency was affected by the corrosion inhibitor concentration. The concentration of the inhibitor in the simulated circulating cooling water can affect the formation rate of the adsorption

Table 5 EIS parameters for carbon steel in simulated circulating cooling water without and with different concentrations of M1 and M2 at 25 °C

Inhibitor	C (mmol L^{-1})	R_s (Ω cm^2)	R_p (Ω cm^2)	CPE		C_{dl} ($\times 10^{-6}$ s^n Ω^{-1} cm^{-2})	η_z (%)
				Y_0 ($\times 10^{-6}$ s^n Ω^{-1} cm^{-2})	n		
Blank	0	2.711 ± 0.071	199.6 ± 3.8	1515.6 ± 4.8	0.81 ± 0.03	686 ± 5	—
M1	0.05	3.057 ± 0.085	441.7 ± 4.7	5988.1 ± 22.7	0.55 ± 0.02	12 365 ± 17	54.81
	0.10	3.212 ± 0.101	546.3 ± 5.2	5260.3 ± 18.8	0.61 ± 0.02	10 447 ± 19	63.46
	0.50	4.643 ± 0.109	735.5 ± 8.8	1680.0 ± 5.1	0.53 ± 0.02	1754 ± 9	72.86
	1.00	5.016 ± 0.106	927.7 ± 10.3	2647.6 ± 4.9	0.53 ± 0.03	6230 ± 10	78.48
	2.50	5.329 ± 0.111	5329 ± 82.1	18 499.0 ± 61.8	0.60 ± 0.02	55 338 ± 43	96.25
M2	0.05	4.196 ± 0.100	484.0 ± 4.4	3991.2 ± 11.7	0.60 ± 0.04	3230 ± 11	58.76
	0.10	3.925 ± 0.087	639.5 ± 7.1	1452.4 ± 6.8	0.48 ± 0.02	1370 ± 7	68.79
	0.50	3.640 ± 0.073	742.8 ± 10.7	3527.0 ± 9.2	0.53 ± 0.02	8200 ± 17	73.13
	1.00	5.657 ± 0.102	1046.0 ± 13.8	21 994.0 ± 68.8	0.63 ± 0.04	110 409 ± 85	80.92
	2.50	5.430 ± 0.108	23 552 ± 111.3	12 988.0 ± 44.1	0.58 ± 0.02	41 534 ± 31	99.15

film layer; therefore, the corresponding capacitive loop and radius increase with increasing concentration. The formation of the time constant at the intermediate frequency can be observed from the angular phase. According to Fig. 2(c)–(f), one time constant for the curve without inhibitor was observed in the Bode plots. However, the angle phase plot shows the formation of two time constants when the inhibitor was added to simulated circulating cooling water. This is due to the film resistance (R_F) of the corrosion inhibitor formed on the surface of the carbon steel. In Fig. 2(d), the phase angles for uninhibited and inhibited solutions of **M1** were 27.37° at 1.212 Hz, 24.20° at 0.026 Hz, 29.75° at 0.038 Hz, 30.04° at 0.121 Hz, 24.05° at 0.032 Hz, and 51.08° at 0.010 Hz, respectively. In Fig. 2(f), the phase angles for uninhibited and inhibited solutions of **M2** were 27.37° at 1.212 Hz, 27.22° at 0.056 Hz, 20.97° at 0.178 Hz, 23.78° at 0.026 Hz, 45.47° at 0.010 Hz, and 34.55° at 0.010 Hz, respectively.

The electrochemical equivalent circuit that was used to fit the interface electrochemical reaction is shown in Fig. 3, where R_{ct} is the charge transfer resistance, R_f is the film resistance, R_{dl} is the diffuse layer resistance, CPE is the constant phase element, and R_s is the solution resistance.[35] R_p is the polarization resistance ($R_p = R_{ct} + R_f + R_{dl}$) of carbon steel in the absence of inhibitor. It is worth noting that when the simulated circulating cooling water contained no inhibitor, the values of R_F and CPEF were approximately equal to 0. Typically, the R_p value is affected by the electron transfer between the metal and the inhibitor; therefore, the R_p value is associated with corrosion inhibition efficiency.[72,73] For better fitting, a CPE was introduced instead of double-layer capacitors (C_{dl}). The CPE can be defined as follows:[74,75]

$$Z_{CPE} = [Y_0(j\omega)^n]^{-1} \quad (13)$$

where Y_0 refers to the proportionality constant of the CPE, j is the imaginary unit, ω is the angular frequency and n is the phase shift.[35] C_{dl} is equated as below:

$$C_{dl} = Y_0(\omega''_m)^{n-1} \quad (14)$$

where ω''_m represents the angular frequency of impedance.

The electrochemical impedance spectroscopy parameters and the calculated inhibition rate η_z (%) are shown in Table 5. The data analysis shows that the value of R_p increased with increasing inhibitor concentration. This is because increasing the concentration of inhibitor can increase the coverage of the inhibitor on the metal surface. However, as the concentration of inhibitor increases, the CPE value decreases, which indicates that the thickness of C_{dl} increased and the dielectric constant decreased; this indicates that the inhibitor was successfully adsorbed on the carbon steel surface and improved the properties of the electric double layer. The η_z (%) value of **M2** is greater than that of **M1**; therefore, the anti-corrosive effect of **M2** on carbon steel is better than that of **M1**, which is consistent with the potentiodynamic polarization curve and the weight loss measurement results. This may be because the planar structure of the **M2** molecule is smoother, and **M2** is thus more easily adsorbed on the surface of the carbon steel than **M1**. In addition to the difference in raw materials, the solubility of **M2** in the simulated circulating cooling water is stronger than that

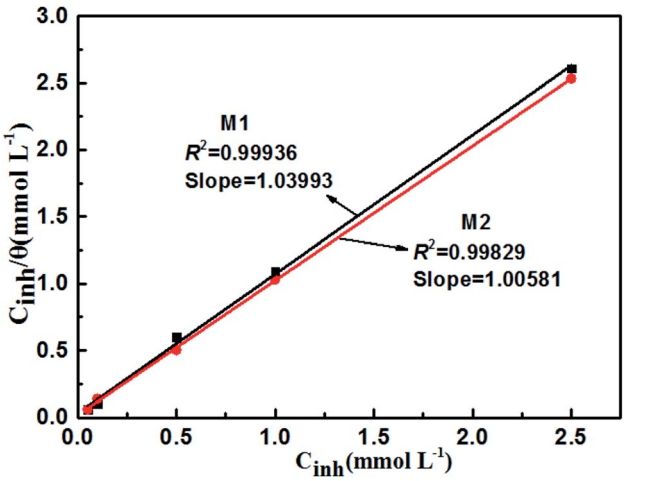

Fig. 4 Langmuir adsorption plots for carbon steel in simulated circulating cooling water containing different concentrations of M1 and M2.

Table 6 Thermodynamic parameters and adsorption parameters of carbon steel in simulated circulating cooling water with **M1** and **M2** at 298 K.

Inhibitor	Temperature (K)	r^2	Slope	K_{ads} (kJ mol^{-1})	ΔG^o_{ads} (kJ mol^{-1})	ΔH^o_{ads} (kJ mol^{-1})	ΔS^o_{ads} (J mol^{-1} K^{-1})
M1	298	0.99955	1.067	937.21	−26.90	−16.95	33.39
M2	298	0.99958	1.026	974.66	−27.02	−17.05	33.46

of **M1**, and a denser protective film is formed on the surface of the carbon steel; this can disrupt electrons and form a closed loop between the metal and the corrosive medium, effectively protecting the metal from corrosion.

3.4 Adsorption isotherm and thermodynamics analysis

Electrochemical studies have confirmed that inhibitor molecules can effectively inhibit the corrosion of carbon steel in simulated circulating cooling water.[35] Through fitting to determine the adsorption isotherm, then choosing the closest r^2 value, the mechanism of the adsorption process of an inhibitor on metal can also be determined. The surface coverage (θ) and concentration (C) of inhibitor molecules on the surface of carbon steel are used to calculate the adsorption constant (K_{ads}), and small changes in coverage can affect the inhibition efficiency. The Langmuir adsorption isotherm is expressed as below:[76,77]

$$\frac{C}{\theta} = \frac{1}{K_{ads}} + C \tag{15}$$

The Langmuir adsorption isotherms of **M1** and **M2** on the surface of carbon steel at various concentrations are shown in Fig. 4. The correlation coefficient (r^2),[78] adsorption constant (K_{ads}), and thermodynamic parameters (ΔG^o_{ads}, ΔH^o_{ads}, ΔS^o_{ads})[79,80] of the adsorption isotherms are shown in Table 6. The following equation correlates K_{ads} and ΔG^o_{ads} as follows (16)–(18):

$$K_{ads} = \frac{1}{55.5} \exp\left(-\frac{\Delta G^o_{ads}}{RT}\right) \tag{16}$$

$$\ln K_{ads} = -\frac{\Delta H^o_{ads}}{RT} + c \tag{17}$$

$$\Delta G^o_{ads} = \Delta H^o_{ads} - T\Delta S^o_{ads} \tag{18}$$

where R, c, and T are the ideal gas constant, integral constant, and absolute temperature (K), respectively. 55.5 is the molar concentration of water (mol L^{-1}).

From Table 6, the r^2 and slope values of inhibitors **M1** and **M2** are very close to 1; this indicates that the adsorption of **M1** and **M2** on the carbon steel surface follows the Langmuir isotherm, and the adsorption type is single-layer.[81,82] If the absolute value of $\Delta G^o_{ads} \geq 20$ kJ mol^{-1}, the inhibitor molecule experiences electrostatic interactions with the metal surface through physisorption. If the absolute value of $\Delta G^o_{ads} \leq$

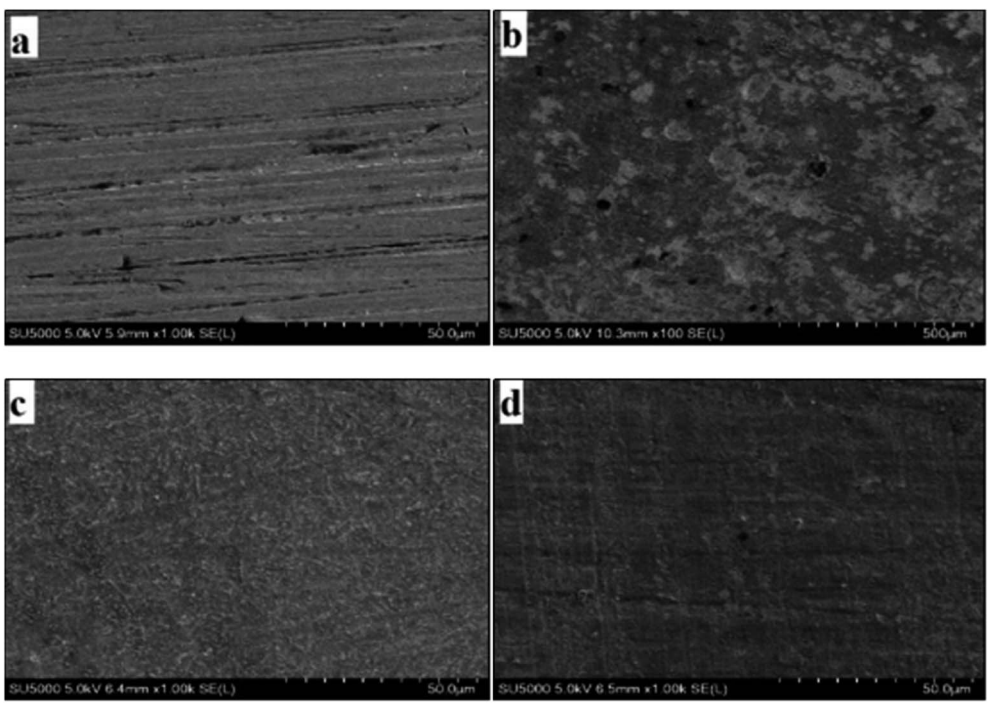

Fig. 5 SEM images of carbon steel surfaces: polished (a) and after 24 h immersion in simulated circulating cooling water without inhibitor (b), with 2.50 mmol L^{-1} **M1** (c) and with 2.50 mmol L^{-1} **M2** (d).

Table 7 The EDS data of mild steel immersed in simulated circulating cooling water in the presence of M1 and M2

Inhibitor	Elemental analysis	Atomic number	Net value (%)	Quality (%)	Normalized quality (%)	Atomic percentage (%)
M1	Oxygen	8	191 120	26.37	27.44	49.67
	Iron	6	224 270	57.93	60.28	31.26
	Carbon	6	11 230	4.51	4.69	11.31
	Sodium	9	9689	3.15	3.28	4.13
	Chromium	24	10 048	1.36	1.42	0.79
	Chlorine	17	14 128	0.88	0.91	0.75
	Magnesium	12	6075	0.59	0.61	0.73
	Sulfur	16	8697	0.52	0.54	0.49
	Silicon	14	5671	0.37	0.38	0.40
	Nitrogen	7	556	0.18	0.19	0.39
	Bromine	35	2084	0.25	0.26	0.09
	Manganese	25	2572	0.80	0.79	0.35
M2	Oxygen	8	117 555	29.02	29.78	51.42
	Iron	26	120 001	54.90	56.34	27.87
	Carbon	6	8570	5.90	6.05	13.93
	Sodium	8	9784	2.34	2.40	2.88
	Chromium	24	6284	1.48	1.52	0.81
	Chlorine	17	9037	0.98	1.01	0.79
	Magnesium	12	3373	0.53	0.55	0.62
	Sulfur	16	5830	0.61	0.62	0.54
	Manganese	25	2731	0.91	0.93	0.47
	Nitrogen	7	265	0.15	0.16	0.31
	Silicon	14	2150	0.23	0.24	0.23
	Bromine	35	1975	0.39	0.40	0.14

40 kJ mol^{-1}, the inhibitor transfers electrons to the metal surface through chemisorption.[83,84] The ΔG^{o}_{ads} values of **M1** and **M2** are −26.90 kJ mol^{-1} and −27.02 kJ mol^{-1}, respectively. This indicates that the inhibitor adsorbs on the steel surface in simulated circulating cooling water by a spontaneous physicochemisorption process.[85,86] Moreover, the negative values for ΔH^{o}_{ads} of **M1** and **M2** indicated that the adsorption is exothermic; therefore, increasing the temperature can reduce the adsorption capacity of the inhibitor molecules on carbon steel.[87] The ΔS^{o}_{ads} values are positive for **M1** and **M2**, which indicates that the inhibitors replace the water molecules adsorbed on the carbon steel surface, increase the chaos of the system, and improve the stability of the protective film.

3.5 SEM and EDS investigations

The morphological information of the carbon steel surface was obtained by SEM analysis. The SEM of carbon steel after 24 h immersion in the simulated circulating cooling water is shown in Fig. 5. The surface of the polished carbon steel was smooth, and the entire surface had some negligible roughness and scratches which were caused by sanding the prepared test piece, as shown in Fig. 5(a). It can be observed that the carbon steel surface (without inhibitor) was severely corroded and oxidized and that corrosion pits appeared, as shown in Fig. 5(b). However, as shown in Fig. 5(c) and (d), when the inhibitor (2.50 mmol L^{-1}) was added to the simulated circulating cooling water, the carbon steel surface become smoother and cleaner because a protective film formed on the carbon steel surface; this can effectively inhibit the corrosion of carbon steel by simulated circulating cooling water. Moreover, the carbon steel in Fig. 5(d) is smoother and flatter than that in Fig. 5(c), which indicates that **M2** possesses better corrosion inhibition ability.

The EDS data of mild steel immersed in simulated circulating cooling water in the presence of **M1** and **M2** are listed in Table 7. The presence of nitrogen on the surface of the carbon steel indicates that the corrosion inhibitor was adsorbed on the surface of the carbon steel. A large number of Cl^{-} ions are present in the simulated circulating cooling water, but only a small amount exists on the surface of the carbon steel; this can be explained by the existence of the etching film layer, which effectively blocks erosion of the carbon steel surface by Cl^{-} ions.

3.6 Quantum chemical calculation analysis

3.6.1 Optimal geometrical structures. The optimal geometries and planar structures of **M1** and **M2** are shown in Fig. 6. The two anthracene rings of the **M2** molecule are coplanar with the glutaraldehyde skeleton, which is related to the fact that the skeleton contains a free-rotating fluorene single bond. The two fluorene rings of the **M1** molecule are in the meta position on the benzene ring; there is large steric hindrance, resulting in non-coplanarity with the benzene ring. In organic chemistry, especially for aromatic compounds, determining the relative activity of each atomic position in an electrophilic or nucleophilic substitution reaction according to front-line orbital theory is an important issue.

In organic chemistry, especially for aromatic compounds, frontier orbital theory (FMO) can be used to determine the relative activity of each atomic position in electrophilic or nucleophilic

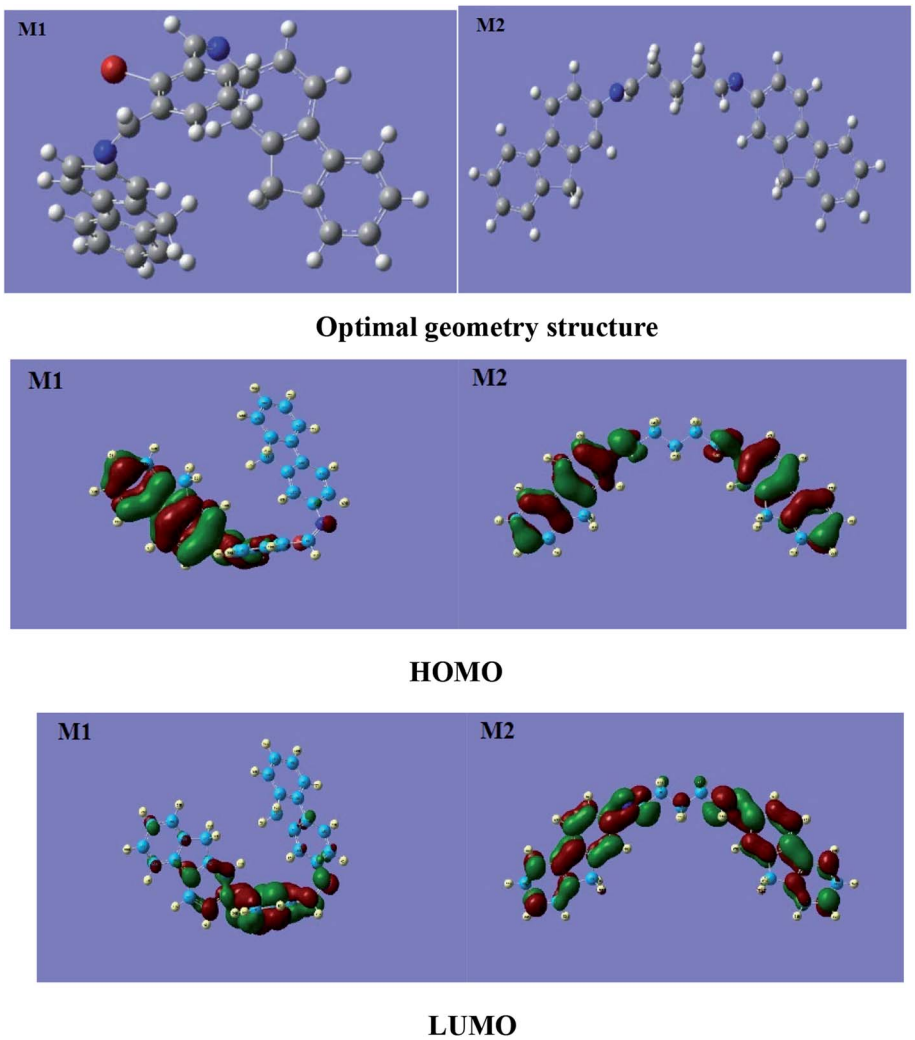

Fig. 6 The optimal geometry structures and HOMO and LUMO orbitals of M1 and M2.

Table 8 Molecular structure parameters of M1 and M2

	Quantum chemical parameter						
Inhibitor	E_{HOMO} (eV)	E_{LUMO} (eV)	ΔE (eV)	χ	η (eV)	σ (eV)	ΔN_{max} (eV)
M1	−6.12	−4.97	1.15	5.55	0.575	1.74	4.81
M2	−6.63	−5.86	0.77	6.25	0.385	2.60	8.12

substitution reactions.[35] The HOMO and LUMO distributions of **M1** and **M2** are shown in Fig. 6. The HOMO of **M1** is mainly distributed on one side of the annulus and the other side of the anthracene ring and is less distributed the intermediate benzene rings; the HOMO of **M2** is mainly distributed on the anthracene rings on both sides and is less distributed the intermediate benzene ring and glutaraldehyde skeleton. HOMOs with high density distributions may become sites for electrophilic attack, which can provide electrons to interact with metallic iron. The LUMO of **M1** is mainly distributed in the middle benzene ring; however, that of **M2** is mainly distributed on the ankle rings on both sides. Regions with large LUMO distributions are likely to be sites for nucleophilic attack, which can enable electrons to interact with metallic iron. However, the electronic donation capacity of **M2** is greater than that of **M1**.

The better corrosion inhibition performance of **M2** than of **M1** may be due to the flatter molecular structure, better symmetry, and higher density distribution of the HOMO and LUMO of **M2**, which enable it to more readily form a protective film on the surface of carbon steel.

3.6.2 Correlation analysis between the structural parameters and corrosion inhibition efficiency. The quantum chemical parameters of the **M1** and **M2** molecules are listed in Table 8. Previous studies have shown that structural parameters such as

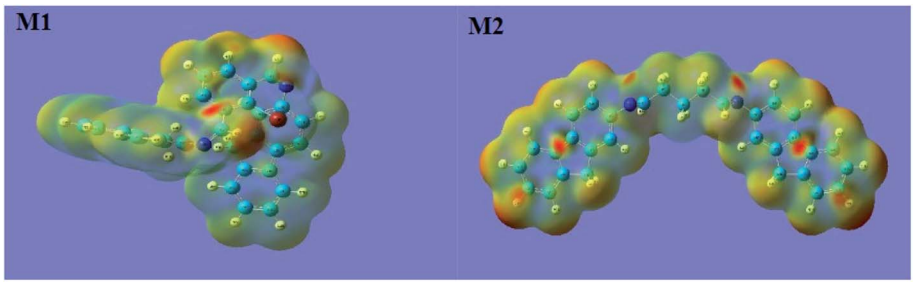

Fig. 7 Fukui function density distribution maps.

the E_{HOMO}, E_{LUMO}, and dipole moment (μ) can be used to explain the adsorption ability of inhibitors on a metal surface.[88,89] As shown in Table 8, the E_{LUMO} value of **M1** is larger than that of **M2**. The greater the E_{LUMO} value, the weaker the ability of the inhibitor to provide an empty orbital to accept d orbital electrons from metallic iron. Therefore, **M2** has higher electron accepting ability and more readily adsorbs on metal surfaces. The gap energy of **M1** is larger than that of **M2**, which indicates that **M2** with a higher inhibition rate can better provide electrons to the empty orbitals of metallic iron. The dipole moment is related to the covalent bond polarity and electron distribution. An inhibitor with a larger μ value is more easily adsorbed on a metal surface. The trend of the dipole moment μ is **M2** > **M1**, which indicates that **M2** has relatively high inhibition efficiency. An inhibitor molecule with greater chemical hardness (η) has greater resistance to charge transfer; the smaller the chemical softness (σ) of the inhibitor molecule, the stronger its ability to accept electrons. The order of the σ values is **M2** > **M1**, and the trend of η is opposite to that of σ. This shows that electron transfer occurs more readily between **M2** and metallic iron than between **M1** and iron. The higher the chemical transfer maximum electron transfer number (ΔN_{max}) of an inhibitor molecule, the higher its tendency to bind to a metal surface. The order of the ΔN_{max} value is **M2** > **M1**; therefore, **M2** has stronger ability to bind to the metal surface than **M1**. Through the analysis of the above structural parameters, it is confirmed that **M2** has greater corrosion inhibition efficiency.

3.6.3 Fukui function analysis. The Fukui function distributions of **M1** and **M2** are shown in Fig. 7. The orange area is the electronic distribution area; the darker the orange, the greater the density of the electron distribution, and the lighter the orange, the smaller the density of the electron distribution. In the molecular structure of **M1**, the f^- function is mostly distributed on the benzene ring and the surrounding *N* atom. In the molecular structure of **M2**, most of the f^- functions are distributed on the ankle rings on both sides. The f^- function distribution is basically consistent with the molecular orbital distribution of the front lines, as shown in Fig. 7. From the above analysis, it was found that the preferred active sites of **M1** and **M2** interacting with the metal surface are the aromatic heterocyclic π system and the C=N functional group, respectively.

3.7 Anticorrosion mechanism analysis

Both these bis-Schiff bases contain two unsaturated –C=N– bonds and heterocyclic functional groups, which provide more adsorption sites and stronger coordination capabilities. The above research shows that the inhibitors **M1** and **M2** have good corrosion inhibition performance for carbon steel in simulated circulating cooling water, which may be due to the physical and chemical adsorption between the inhibitor molecules and the carbon steel surface. The adsorption of corrosion inhibitors on metal surfaces can be summarized as follows: firstly, the corrosion inhibition efficiencies of **M1** and **M2** can be attributed to the existence of electron-rich N atoms and heterocyclic rings in their structures.[90] The unsaturated –C=N– bond in the neutral **M1** and **M2** molecular structures contains a lone pair of electrons, which can form a stable covalent bond with the empty orbital of the Fe atom in the carbon steel; thus, the inhibitors can be absorbed on the surface of the carbon steel. The heterocyclic rings in the compounds have abundant shared π electrons and can interact with the metal surface through polycentric adsorption to form a dense protective film on the carbon steel surface.[91] The simulated circulating cooling water has high salt content, and unsaturated –C=N– bonds can chemically react with metal ions, reducing the substitution reaction between the carbon steel surface and other active metal ions. Secondly, because the simulated circulating cooling water contains a certain amount of H^+, H^+ is adsorbed on the carbon steel surface and is positively charged; under the action of Coulomb forces, anions such as Cl^- are preferentially adsorbed on the carbon steel surface. Hence, the adsorption of the carbon steel surface is selectively converted from negative charge to positive charge,[48] and the adsorption of protonated **M1**, **M2** molecules on the carbon steel surface is promoted by electrostatic action. In summary, **M1** and **M2** molecules are adsorbed on the carbon steel surface by physical and chemical interactions to form a dense protective film in the simulated circulating cooling water, thereby effectively preventing the corrosion of the carbon steel by the corrosive medium.

4. Conclusions

In this paper, two new 2-aminofluorene bis-Schiff base compounds, **M1** and **M2**, were designed, successfully synthesized, and characterized.

The weight loss and electrochemical measurement results showed that **M1** and **M2** exhibit maximum inhibition efficiency at concentrations of 2.50 mmol L^{-1} at 25 °C.

The SEM studies confirmed that **M1** and **M2** successfully formed films on the surface of carbon steel.

The negative values of ΔG^{o}_{ads} confirmed that the adsorption processes for **M1** and **M2** are spontaneous physicochemisorption processes that obey Langmuir adsorption isotherms.

All experimental and theoretical results supported that the bis-Schiff base inhibitor **M2** possesses higher corrosion inhibition efficiency than **M1**.

Conflicts of interest

There are no conflicts of interest to declare.

Acknowledgements

We thank the National Nature Science Foundation of China (61661014), Nature Science Foundation of Guangxi Province (No. 2018GXNSFAA281198, 2018GXNSFBA281135, 2018GXNSFAA294042) and Guangxi Zhuang Autonomous Region and the special funding for distinguished expert, Guangxi One Thousand Young and Middle-aged College and University Backbone Teachers Cultivation Program and Guangxi Science and Technology Base and Talents Special Project (2018AD09002).

References

1 M. V. Biezma and J. R. S. CristãBal, *Corros. Eng. Sci. Technol.*, 2013, **40**, 344–352.
2 T. Miroshnikova and N. Kuchugin, *Procedia Economics and Finance*, 2015, **24**, 426–434.
3 S. Shahabi, S. Hamidi and J. B. Ghasemi, *J. Mol. Liq.* , 2019, **285**, 626–639.
4 Y. M. Panchenko and A. I. Marshakov, *Corros. Sci.*, 2016, **109**, 217–229.
5 D. J. Carbonell, A. García-Casas and J. Izquierdo, *Corros. Sci.*, 2016, **111**, 625–636.
6 H. R. Bhat, U. P. Singh and P. Gahtori, *RSC Adv.*, 2013, **3**, 2942.
7 S. Chimenti, J. M. Vega and M. Aguirre, *J. Coat. Technol. Res.*, 2017, **14**, 829–839.
8 H. B. Choe, H. S. Lee and J. H. Shin, *Materials*, 2014, **7**, 7722–7736.
9 P. Han, C. Chen and W. Li, *J. Colloid Interface Sci.*, 2018, **516**, 398–406.
10 I. Ahamad, R. Prasad and M. A. Quraishi, *Corros. Sci.*, 2010, **52**, 1472–1481.
11 L. Fu, Y. Fei and Z. Bo, *Russ. J. Appl. Chem.*, 2018, **91**, 499–509.
12 X. Luo, X. Pan and Y. Song, *Corros. Sci.*, 2017, **125**, 139–151.
13 H. Peng, C. Chen and H. Yu, *Corros. Sci.*, 2016, **112**, 128–137.
14 A. A. Golovanov, S. A. Dan'Kov and S. A. Sokov, *Chem. Heterocycl. Compd.*, 2019, **55**, 1–4.
15 S. Vikneshvaran and S. Velmathi, *Mater. Corros.*, 2018, **69**, 1084–1094.
16 M. Abdel-Shakour, W. A. El-Said and I. M. Abdellah, *J. Mater. Sci.: Mater. Electron.*, 2019, **30**, 5081–5091.
17 N. Kovačević and A. Kokalj, *Mater. Chem. Phys.*, 2012, **137**, 331–339.
18 M. Goyal, S. Kumar and I. Bahadur, *J. Mol. Liq.*, 2018, **256**, 565–573.
19 M. J. Garciaramirez, G. F. Dominguez Patiño and J. G. Gonzalezrodriguez, *Adv. Mater. Phys. Chem.*, 2016, **6**, 9–20.
20 C. Verma, J. Haque and E. E. Ebenso, *Results Phys.*, 2018, **9**, 100–112.
21 N. M. E. Basiony, A. Elgendy and H. A. Nady, *RSC Adv.*, 2019, **9**, 10473–10485.
22 X. Yang, F. Li and W. Zhang, *RSC Adv.*, 2019, **9**, 10454–10464.
23 C. Küstü, K. C. Emregül and O. Atakol, *Corros. Sci.*, 2007, **49**, 2800–2814.
24 P. Roy, A. Pal and D. Sukul, *RSC Adv.*, 2014, **4**, 10607.
25 M. A. Deyab, *Electrochim. Acta*, 2016, **202**, 262–268.
26 L. Fang, L. ü. Yucui and J. Guofei, *China Pet. Process. Petrochem. Technol.*, 2017, **19**, 21–32.
27 R. Liang, J. Li and M. Liu, *Colloids Surf., B*, 2018, **172**, 1–9.
28 G. Petkova, E. Sokolova and S. Raicheva, *Br. Corros. J.*, 1996, **31**, 55–60.
29 K. Rahmani, *Appl. Therm. Eng.*, 2017, **114**, 849–856.
30 Y. M. Chen, C. X. Sun and H. W. Xu, *Adv. Mater. Res.*, 2014, **881–883**, 604–609.
31 A. C. Balaskas, M. Curioni and G. E. Thompson, *Surf. Interface Anal.*, 2015, **47**, 1029–1039.
32 Y. Liu, Y. Zhang and J. Yuan, *Eng. Failure Anal.*, 2014, **45**, 225–233.
33 J. Kao and R. Chen, *Curr. Nanosci.*, 2012, **8**, 1–2.
34 X. Sang, Z. Wang and J. Li, *ChemistrySelect*, 2018, **3**, 7358–7362.
35 M. Murmu, K. S. Saha and C. N. Murmu, *Corros. Sci.*, 2019, **146**, 134–151.
36 S. S. Chen, A. Singh and Y. Q. Wang, *Int. J. Electrochem. Sci.*, 2017, **12**, 782–796.
37 D. B. Celepci, N. Korkmaz and S. T. Astley, *J. Struct. Chem.*, 2019, **60**, 151–158.
38 L. Fang, L. Xianhui and Y. Wei, *Desalination*, 2013, **313**, 18–27.
39 Y. J. Yu, D. S. Byeon and Y. J. Shin, *CrystEngComm*, 2017, **19**, 6731–6735.
40 H. Matsubara, K. Mizuno and Y. Takeuchi, *Jpn. J. Appl. Phys.*, 2013, **52**, 08JE17.
41 G. Georg, L. Alberto and J. Rafael Sendra, *J. Comput. Appl. Math.*, 2016, **300**, 119–133.
42 B. Stuart, *Infrared Spectroscopy: Fundamentals and Applications*, Wiley, 2004, ISBN no. 978-0-470-85428-0.
43 M. Beniken, M. Driouch and M. Sfaira, *J. Bio. Tribo-Corros.*, 2018, **4**, 38–51.
44 H. M. Abd Ellateef, V. M. Abbasov and L. I. Aliyeva, *J. Surface. Interfac. Mater*, 2013, **1**, 4–14.
45 N. Al-Baker, R. Shawabkeh and R. Rihan, *Br. Corros. J.*, 2013, **46**, 767–776.
46 V. V. Torres, R. S. Amado and C. F. D. Sá, *Corros. Sci.*, 2011, **53**, 2385–2392.
47 G. Liang, X. Peng and X. Luyao, *J. Mater. Eng. Perform.*, 2013, **22**, 3043–3048.
48 C. X. Liang, Z. Liu and Q. Q. Liang, *J. Mol. Liq.*, 2019, **277**, 330–340.

49 K. V. Rybalka, L. A. Beketaeva and A. D. Davydov, *Russ. J. Electrochem.*, 2018, **54**, 456–458.
50 S. Yesudass, L. O. Olasunkanmi and I. Bahadur, *J. Taiwan Inst. Chem. Eng.*, 2016, **64**, 252–268.
51 H. Lgaz, K. S. Bhat and R. Salghi, *J. Mol. Liq.*, 2017, **238**, 71–83.
52 A. Ehsani, M. G. Mahjani and R. Moshrefi, *RSC Adv.*, 2014, **4**, 20031.
53 S. Issaadi, T. Douadi and A. Zouaoui, *Corros. Sci.*, 2011, **53**, 1484–1488.
54 S. Shirin and N. Parviz, *Int. J. Electrochem. Sci.*, 2017, **12**, 2628–2646.
55 T. Peme, L. Olasunkanmi and I. Bahadur, *Molecules*, 2015, **20**, 16004–16029.
56 H. E. Yi, Y. Q. Zhou and R. R. Yang, *Mod. Chem. Ind.*, 2016, **15**, 37–42.
57 E. M. Zayed, A. M. M. Hindy and G. G. Mohamed, *Appl. Organomet. Chem.*, 2018, **32**, 3952–3968.
58 F. Cuenú, J. Londoñosalazar and J. E. Torres, *J. Mol. Struct.*, 2018, **1152**, 163–176.
59 M. M. A. El-Sukkary, I. Aiad and A. Deeb, *Liq. Fuels Technol.*, 2010, **28**, 1158–1169.
60 Z. Demircioğlu, C. A. Kastas and O. Büyükgüngör, *Spectrochim. Acta, Part A*, 2015, **139**, 539–548.
61 Y. Ma, L. Jin and D. Zhao, *RSC Adv.*, 2014, **4**, 17262–17264.
62 C. L. Murulana, M. M. Kabanda and E. E. Ebenso, *J. Mol. Liq.*, 2016, **215**, 763–779.
63 A. Miodek, E. Regan and N. Bhalla, *Sensors*, 2015, **15**, 25015–25032.
64 P. Tsakiropoulos, *Materials*, 2018, **11**(1), 69.
65 M. Franco-Pérez, J. L. Gázquez and P. W. Ayers, *J. Chem. Phys.*, 2015, **143**, 154103.
66 K. Ansari, M. Quraishi and A. Singh, *Corros. Sci.*, 2014, **79**, 5–15.
67 J. Jennane, M. E. Touhami and S. Zehra, *Mater. Chem. Phys.*, 2019, **227**, 200–210.
68 D. S. Carvalho, C. J. B. Joia and O. R. Mattos, *Corros. Sci.*, 2005, **47**, 2974–2986.
69 D. I. Zhukhovitskii, O. F. Petrov and T. W. Hyde, *New J. Phys.*, 2015, **17**, 846–861.
70 W. Yang and W. J. Mortier, *J. Am. Chem. Soc.*, 1986, **108**, 5708–5711.
71 M. Migahed, A. Al-Sabagh, E. Khamis and E. Zaki, *J. Mol. Liq.*, 2015, **212**, 360–371.
72 T. C. Liu, Q. Y. Hu and X. H. Li, *J. Mater. Chem. A*, 2019, **7**, 20911–20918.
73 H. Han, S. J. Park, J. S. Jang, *et al.*, *ACS Appl. Mater. Interfaces*, 2013, **5**, 3441–3448.
74 P. Thiraviyam and K. Kannan, *Arabian J. Sci. Eng.*, 2013, **38**, 1757–1767.
75 J. H. Shim, S. J. Lee and H. Gim, *Mol. Med. Rep.*, 2016, **14**, 3908–3916.
76 C. H. Hsu and F. Mansfeld, *Corros. Sci.*, 2001, **57**, 747–753.
77 L. O. Olasunkanmi, B. P. Moloto and I. O. Obot, *J. Mol. Liq.*, 2018, **252**, 62–74.
78 S. M. A. Hosseini and M. J. Bahrami , *Mater. Corros.*, 2015, **86**, 166–871.
79 M. V. Ozhukil, M. Roopesh and S. Alwarappan, *Langmuir*, 2018, **34**, 5374–5380.
80 Z. Cui, J. Zhang and Y. Xue, *Langmuir*, 2018, **34**, 3197–3206.
81 Y. P. Khodyrev, E. S. Batyeva and E. K. Badeeva, *Corros. Sci.*, 2011, **53**, 976–983.
82 H. T. Dang, M. D. S. Dias and A. Liebsch, *Phys. Rev. B*, 2016, **93**, 115–123.
83 X. Q. Hu and C. H. Liang, *Mater. Chem. Phys.*, 2008, **110**, 285–290.
84 P. Thanapackiam, S. Rameshkumar and S. S. Subramanian, *Mater. Chem. Phys.*, 2016, **174**, 129–137.
85 P. C. Okafor and Y. Zheng, *Corros. Sci.*, 2009, **51**, 850–859.
86 P. Roy, S. K. Saha, P. Banerjee, S. Dey and D. Sukul, *Res. Chem. Intermed.*, 2017, **43**, 4423–4444.
87 L. C. Murulana, M. M. Kabanda and E. E. Ebenso, *J. Mol. Liq.*, 2016, **215**, 763–779.
88 A. Döner, R. Solmaz and M. Özcan, *Corros. Sci.*, 2011, **53**, 2902–2913.
89 F. J. Rodríguez-Gómez, M. P. Valdelamar and A. E. Vazquez, *J. Mol. Struct.*, 2019, **1183**, 168–181.
90 P. Muthukrishnan, B. Jeyaprabha, P. Tharmaraj and P. Prakash, *Res. Chem. Intermed.*, 2015, **41**, 5961–5984.
91 S. P. Fakrudeen, H. C. A. Murthy and V. B. Raju, *J. Chil. Chem. Soc.*, 2012, **57**, 1364–1371.

